Pergamon

Int. J. Solids Structures Vol. 35, No. 15, pp. 1793–1811, 1998

0020–7683/98 $19.00 + .00

PII: S0020–7683(97)00152–2

ANALYSIS OF COMPOSITE LAMINATES WITH MULTIPLE FASTENERS

E. MADENCI, S. SHKARAYEV, B. SERGEEV
Department of Aerospace and Mechanical Engineering, The University of Arizona, Aero Bldg. 16, Tucson, Arizona 85721, U.S.A.

D. W. OPLINGER and P. SHYPRYKEVICH
Airframe Structures Section AAR-431, DoT/FAA Technical Center, Atlantic City International Airport, New Jersey 08405, U.S.A.

(*Received* 10 *December* 1996; *in revised form* 23 *May* 1997)

Abstract—Fatigue- and fracture-related cracks are to be expected with the large number of fasteners present in aircraft structures. Therefore, contact stresses around the fastener holes and stress intensity factors associated with edge cracks are critical concerns in damage-tolerant designs. Mechanical joints consisting of many fasteners with a staggered pattern further complicate the already rather complex analysis for single-fastener joints. Load distribution among the fasteners significantly influences the failure load of multi-fastener joints. Most existing analyses are confined to single-fastener joints, and the data available for multi-fastener joints are rather limited. Very few experimental and/or analytical/numerical investigations of contact stresses for mechanical joints with staggered fasteners exist in the literature. Therefore, the accurate prediction of contact stresses (load distribution) and stress intensity factors associated with edge cracks is essential for the reliable design of such mechanical joints. This study concerns the development of an analytical methodology, based on the boundary collocation technique, to determine the contact stresses and stress intensity factors required for strength and life prediction of bolted joints with many fasteners. It provides an analytical capability for determining the contact stresses in mechanically fastened composite laminates while capturing the effects of finite geometry, presence of edge cracks, interaction among fasteners, material anisotropy, fastener flexibility, fastener-hole clearance, friction between the pin and the laminate, and by-pass loading. Also, it permits determination of the fastener load distribution, which significantly influences the failure load of a multi-fastener joint. © 1998 Elsevier Science Ltd.

INTRODUCTION

Mechanical fasteners provide the primary means for transferring load among components in the construction of aircraft structures. However, they are associated with high stress concentrations leading to failure modes of net-section, bearing, and shear-out in composites and to crack initiation from the hole boundary in metals. Therefore, assessment of the stresses around the fastener holes and the stress intensity factors associated with edge cracks is critical for damage-tolerant designs. Because of the presence of unknown contact stresses and the contact region between the fastener and the laminate, the analysis of a pin-loaded hole is considerably more complex than that of a traction-free hole. In the presence of cracks, both the strength and crack growth depend upon the stress field at the tip of the crack, which is characterized by the stress intensity factors. The distribution of the contact stresses along the boundary is critical for determining the stress intensity factors. Therefore, accurate determination of the contact stresses and the stress intensity factors associated with such loaded holes in mechanically fastened joints is essential to reliable strength evaluation and failure prediction.

The stress state in a mechanical joint is dependent primarily on the geometry of the bolted laminates, loading conditions, material anisotropy, fastener-hole clearance, fastener flexibility, and the friction between the fastener and the laminate. Mechanical joints consisting of many fasteners with a staggered pattern further complicate the already rather complex analysis for single-fastener joints. Load distribution among the fasteners significantly influences the failure load of multi-fastener joints. The presence of the unknown contact stress distribution and the contact region between the fastener and the laminates

and the interaction among the fasteners result in a complex nonlinear problem. In the case of multi-fastener joints, the commonly accepted approach is based on first determining the load distribution among the fasteners in order to identify the critical (most highly loaded) fastener for a subsequent single-fastener analysis for local stress distribution. However, this type of analysis disregards the interaction among the fasteners located in close proximity to each other.

Although a considerable amount of work on the behavior of composite joints with a single fastener has been reported in the literature, experimental and analytical/numerical consideration of multi-fastener joints is rather limited. The majority of the experimental investigations are concerned with two fasteners in tandem. Rowlands *et al.* (1982), and Hyer and Liu (1984) obtained the isochromatic fringe patterns in their investigations of such a configuration. However, they could not determine the spatial distribution of the contact stresses around the pin-loaded holes from the photoelastic measurements. Experimental investigations concerning complex fastener patterns report only the failure load. These results indicate that the failure load per fastener decreases with increasing complexity, i.e. the joint efficiency decreases with an increasing number of fasteners.

Except for a study by Griffin *et al.* (1994), analytical/numerical models concerning the stress and load distribution of mechanical joints with staggered fasteners are non-existent because of the required complexity. By utilizing the appropriate symmetry conditions, Griffin *et al.* considered a row of staggered fasteners through a finite element model with gap elements. In the case of mechanical joints with fasteners in tandem and/or parallel to each other. Xiong and Poon (1994) and Eriksson *et al.* (1995) presented results based on a two-stage analysis. The analytical approach by Xiong and Poon utilizes a variational formulation in conjunction with complex stress functions introduced by Lekhnitskii (1968) for anisotropic plates with a single hole. This approach considers each laminate of the joint separately. Their coupling is achieved through the fastener displacements, which are permitted only in the direction of loading. In this approach, the presence of multiple fasteners is included in an average sense because of the limitation of the variational formulation. The first stage of their analysis provides the local deformation along the hole boundaries of one of the laminates subjected to the external boundary conditions, and the prescribed cosinusoidal bearing fastener deflections are imposed as displacement constraints in the subsequent analysis to determine the contact stresses (fastener loads) and the contact region in the second laminate. Subsequently, these fastener loads are imposed as prescribed cosinusoidal bearing stress for the first stage of the analysis, and the iterative process continues until constraint conditions are satisfied.

The approach by Eriksson *et al.* (1995) first establishes the fastener load distribution to identify the most critical fastener site and then solves for the stress distribution around this fastener hole. The fasteners and holes are not modeled explicitly in the first stage of the finite element analysis, however, they are represented by spring elements that are connected to node points on the lower and upper laminates. While disregarding the influence of the contact stress on the interaction among the fasteners, the subsequent finite element analysis provides the contact stresses and the contact region for a pin-loaded hole.

In addition to the aforementioned analyses, Oplinger (1978) determined the stress distribution in an orthotropic laminate subjected to a uniform load normal to a single row of pin-loaded holes under certain simplifying assumptions of symmetry and periodicity. In the case of two fasteners in tandem, Rowlands *et al.* (1982) determined the contact stresses by using an incremental finite element analysis with an iterative solution procedure. They discussed the significance of variations in load distribution among bolts, friction, material properties, spacing, pin-hole clearance and end distance on the contact stresses. Also, Oplinger and Gandhi (1974) discussed the effects of multiple fasteners in parallel or series on the mechanical joint design.

In the presence of radial edge cracks emanating from the boundary of the hole, the load exerted by the fastener on the edge of the hole results in combined stress intensity factors for the opening and sliding modes, K_I and K_{II}, respectively. A non-zero K_{II} occurs due to non-symmetrical (around the crack line) deformation, even though friction (and tangential contact stresses) may be zero. Tangential contact stresses are present only with

friction. The transmission of these unknown contact stresses through an unknown contact region and the presence of radial cracks render this problem highly nonlinear. Because of the important of this subject, this problem has been investigated analytically and numerically. Except for the finite element modeling conducted by Chiang and Rowlands (1991), none of the other analytical models are satisfactory. The main discrepancy among these analytical models is that the distributions of the contact stresses and the contact region are assumed to be known *a priori*. Therefore, they cannot be used to examine the effect of pin-hole clearance and friction between the fastener and the hold boundary on the stress intensity factors.

There are no experimental and analytical/numerical investigations of multi-fastener joints with edge cracks in the literature. Also, it is apparent that analytical investigations of bolted joints consisting of two or more fasteners without any symmetry requirements are limited and inadequate. Furthermore, the stress intensity factors for multi-fastener joints with potential edge cracks are needed in order to employ damage-tolerant design concepts during the design process. Thus, a comprehensive analysis methodology is required in order to predict the contact stresses (load transferred by each fastener) and the stress intensity factors associated with edge cracks in mechanical joints with arbitrarily located fasteners. Although finite element analysis is useful in the evaluation of a complex joint geometry, it is not suitable for iterative design calculations for optimizing laminate construction in the presence of single and multiple fasteners. Therefore, this study is concerned with the development of an analytical/numerical approach for the assessment of the contact stresses, the contact regions, and the stress intensity factors for mechanical joints consisting of arbitrarily located multiple fasteners with or without edge cracks.

PROBLEM STATEMENT

As shown in Fig. 1, the upper and lower laminates, representing two different regions, joined with K numbers of fasteners are subjected to uniform normal stresses, $\sigma^1{}_*$ and $\sigma^2{}_*$, respectively. The regions representing the laminates consist of sub-domains, in each of which is a fastener. The super- and subscripts refer to the regions and sub-domains, respectively. The length and width of the kth rectangular sub-domain in the pth region are denoted by L_k^p and H_k^p, respectively, with their corresponding thickness, t_k^p. The position of the fastener in relation to the boundaries of the sub-domains is specified by l_k^p and h_k^p. As illustrated in Fig. 2, the hole radius, a_k, which is slightly larger than that of the fastener, R_k, in the kth sub-domain, leads to a clearance of λ_k. The hole and fastener radii remain the same for the kth sub-domain of each region.

Cartesian (x_k, y_k) and polar (r_k, θ_k) coordinate systems, whose origins are located at the center of the fastener hole in the kth sub-domain, are utilized in the statement of the boundary conditions. As the joint is subjected to external loading, each fastener exerts the loading on the hole boundary through the contact region of the lower and upper laminates. As shown in Fig. 2, this region, whose extent is not known, consists of no-slip and slip

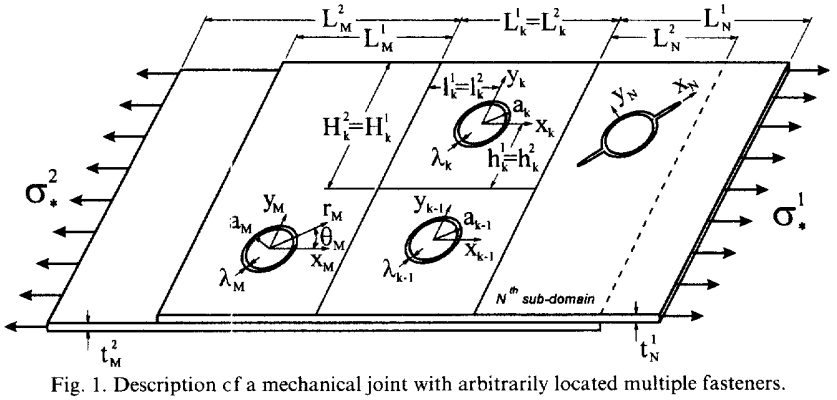

Fig. 1. Description of a mechanical joint with arbitrarily located multiple fasteners.

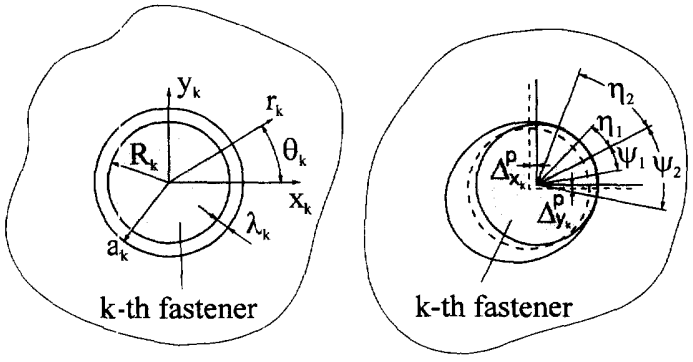

Fig. 2. Position of a fastener before and after loading in relation to the hole boundary.

zones because of the presence of friction between the hole boundary and the fastener. The angles η_{1k}^p and ψ_{1k}^p, and η_{2k}^p and ψ_{2k}^p define the extent of the no-slip and slip zones. The unknown load exerted by the kth fastener in the pth region is composed of F_{xk}^p and F_{yk}^p along the x_k and y_k directions. In each sub-domain, the fastener forces exerted on the lower and upper laminates are equal and opposite to each other. The magnitude of the fastener forces are dependent on the relative displacement of the lower and upper laminates. Their relative displacement consists of the deformation of the hole boundaries and the fastener deflections. At the intersection of the hole boundary and the line of action for the fastener force in the kth sub-domain belonging to the pth region, the components of the local displacements are represented by Δ_{xk}^p and Δ_{yk}^p along the x_k and y_k directions, respectively. The kth fastener compliance, S_k, linearly relates the fastener deflection to the fastener force. Although the physical interpretation of the fastener compliance is obvious, its value depends on the assumptions involved while modeling the fastener as a short beam. In this study, the approach presented by Xiong ad Poon (1994) is adopted to calculate the compliance of the k fastener

$$S_k = \left(\frac{2R_k}{t_k^1}\right)^2 \frac{(t_k^1 + k_k^2)^3}{12E_kI_k}\left[1 + \frac{12\kappa_k E_k I_k}{G_k A_k (t_k^1 + t_k^2)^2}\right] \tag{1}$$

where the shear coefficient parameter, κ, has a value of 1.33 and E_kI_k are G_kA_k, the bending and shear rigidity, respectively.

The boundary conditions along the fastener hole can be stated as

$$u_k^p(a_k, \theta_k) = (\Delta_{xk}^p + \delta_{p2} S_k F_{xk}^p)\cos\theta_k + (\Delta_{yk}^p + \delta_{p2} S_k F_{yk}^p)\sin\theta_k - \lambda_k \quad \theta_k \in [-\psi_{2k}^p, \eta_{2k}^p] \tag{2a}$$

$$v_k^p(a_k, \theta_k) = (\Delta_{xk}^p + \delta_{p2} S_k F_{xk}^p)\sin\theta_k + (\Delta_{yk}^p + \delta_{p2} S_k F_{yk}^p)\cos\theta_k \quad \theta_k \in [-\psi_{1k}^p, \eta_{1k}^p] \tag{2b}$$

$$\tau_k^p(a_k, \theta_k) = f|\sigma_k^p(a_k, \theta_k)| \quad \theta_k \in [\eta_{1k}^p, \eta_{2k}^p], \quad \theta_k \in [-\psi_{1k}^p, -\psi_{2k}^p] \tag{2c}$$

$$\sigma_k^p(a_k, \theta_k) = \tau_k^p(a_k, \theta_k) = 0 \quad \theta_k \in \eta_{2k}^p, -\psi_{2k}^p \tag{2d}$$

where δ_{p2} is the Kronecker delta with $p = 1, 2$. In the no-slip zone, both the normal and tangential displacement components, u_p^k and v_p^k, respectively, of the hole boundary are equal to those of the fastener. In the slip zone, the shear stress, τ_k^p, develops and the difference in the normal displacement components of the hole boundary and that of the fastener vanishes. The shear stress is related to the normal stress, σ_k^p, by adopting a Coulomb friction model with coefficient of friction, f. The angles η_{1k}^p and ψ_{1k}^p, and η_{2k}^p and ψ_{2k}^p, as well as the components of the fastener displacement, Δ_{xk}^p and Δ_{yk}^p, and force, F_{xk}^p and F_{yk}^p, are determined as part of the solution for each region by imposing the following constraints:

$$a_k \int_0^{2\pi} [-\sigma_k^p(a_k, \theta_k) \cos\theta_k + \tau_k^p(a_k, \theta_k) \sin\theta_k] \, d\theta_k + F_{xk}^p = 0$$

$$a_k \int_0^{2\pi} [-\sigma_k^p(a_k, \theta_k) \sin\theta_k + \tau_k^p(a_k, \theta_k) \cos\theta_k] \, d\theta_k + F_{yk}^p = 0$$

$$\sigma_k^p(a_k, \theta_k) < 0 \quad \theta_k \in [-\psi_k^p, \eta_{2k}^p] \quad \sigma_k^p(a_k, -\psi_{2k}^p) = \sigma_k^p(a_k, \eta_{2k}^p) = 0$$

$$|\tau_k^p(a_k, -\eta_{1k}^{p-}) - \tau_k^p(a_k, \eta_{1k}^{p+})| = 0 \quad |\tau_k^p(a_k, -\psi_{1k}^{p-}) - \tau_k^p(a_k, \psi_{1k}^{p+})| = 0 \tag{3}$$

in which the superscripts $-$ and $+$ denote the angles associated with the no-slip and slip zones, respectively. Also, the condition of equal and opposite kth fastener forces in each region is enforced as

$$F_{xk}^1 + F_{xk}^2 = 0 \quad \text{and} \quad F_{yk}^1 + F_{yk}^2 = 0. \tag{4}$$

Imposing the boundary and continuity conditions and the additional constraints results in a nonlinear load transfer problem.

SOLUTION METHOD

The solutions to the contact stresses and the extent of the contact region, as well as the components of the fastener displacement and the force exerted by the fastener in the lower and upper laminates, are obtained by employing the boundary collocation technique. This method utilizes the complex analytic functions introduced by Lekhnitskii (1968) for analyzing the simply-connected anisotropic domains, which are infinite in extent. Applying the concept of the modified mapping collocation (MMC) technique introduced by Bowie and Neal (1970) to these analytic functions permits the imposition of the boundary conditions associated with a finite domain. In this domain, the field equations are satisfied exactly, however, the boundary conditions are satisfied approximately at the collocation points. In the case of a region with multiple internal boundaries, as shown in Fig. 3, the region is partitioned into simply-connected sub-domains. The continuity of the displacement and traction components is enforced at the collocation points common to the boundaries of the sub-domains. The external boundary of the kth sub-domain, B_k, is defined with respect to the Cartesian coordinates (x_k, y_k). As shown in Fig. 3, the origin of this coordinate system coincides with the center of the internal domain bounded by Γ_κ. Its

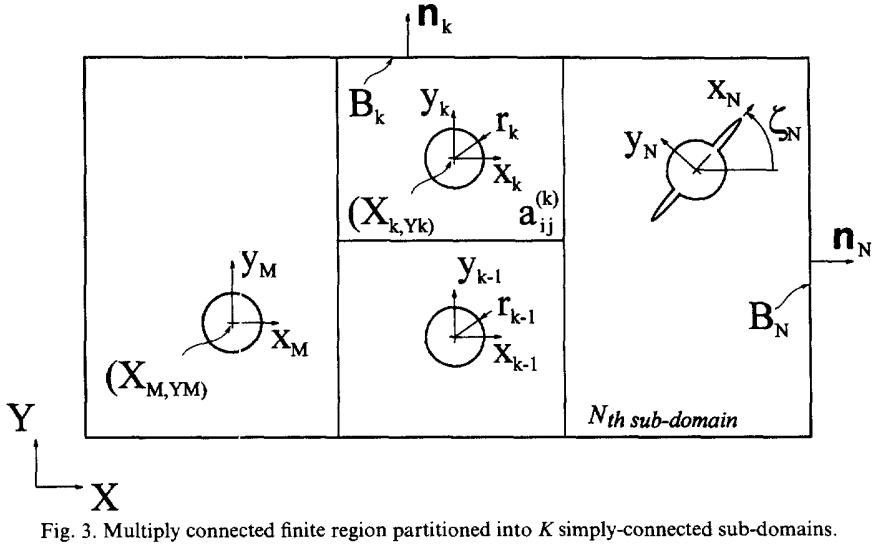

Fig. 3. Multiply connected finite region partitioned into K simply-connected sub-domains.

origin is located at (X_k, Y_k) with an orientation angle of ζ_k in reference to the global coordinate system (X, Y).

As shown in Fig. 4, a region partitioned into sub-domains containing "external", "internal" and "common" types of collocation points associated with the external, internal and common boundaries of the sub-domains, respectively. Prescribed boundary conditions of stress and/or displacement components are imposed at the "external" and "internal" collocation points. The continuity of the stress and displacement components is enforced at the "common" collocation points.

Based on Lekhnitskii's (1968) solution method within the two-dimensional theory of elasticity concerning anisotropic laminates, the normal and tangential stress and displacement components at the jth collocation point of the kth sub-domain in a region (Fig. 4) are expressed in matrix form as

$$\begin{aligned} \boldsymbol{\sigma}_k(x_k^j, y_k^j) &= 2\,\mathrm{Re}\,[\mathbf{s}_k \quad \boldsymbol{\mu}_k \quad \boldsymbol{\phi}_k' \quad \mathbf{l} \quad \boldsymbol{\chi}_k] \\ \mathbf{u}_k(x_k^j, y_k^j) &= 2\,\mathrm{Re}\,[\mathbf{t}_k \quad \mathbf{p}_k \quad \boldsymbol{\phi}_k \quad \mathbf{m} \quad \boldsymbol{\chi}_k] \end{aligned} \tag{5}$$

where the vectors $\boldsymbol{\sigma}_k$ and $\mathbf{u}_k$ are defined as

$$\boldsymbol{\sigma}_k = \begin{Bmatrix} \sigma \\ \tau \end{Bmatrix}_k \quad \text{and} \quad \mathbf{u}_k = \begin{Bmatrix} u \\ v \end{Bmatrix}_k \tag{6}$$

with σ, τ and u, v representing the normal and tangential stress and displacement components, respectively. The transformation matrices, $\mathbf{s}_k$ and $\mathbf{t}_k$, are given by

$$\mathbf{s}_k = \begin{bmatrix} \cos^2(\mathbf{n}_k^j, x_k) & \sin^2(\mathbf{n}_k^j, x_k) & 2\cos(\mathbf{n}_k^j, x_k)\sin(\mathbf{n}_k^j, x_k) \\ -\cos(\mathbf{n}_k^j, x_k)\sin(\mathbf{n}_k^j, x_k) & \cos(\mathbf{n}_k^j, x_k)\sin(\mathbf{n}_k^j, x_k) & (\cos^2(\mathbf{n}_k^j, x_k) - \sin^2(\mathbf{n}_k^j, x_k)) \end{bmatrix}$$

and

$$\mathbf{t}_k = \begin{bmatrix} \cos(\mathbf{n}_k^j, x_k) & \sin(\mathbf{n}_k^j, x_k) \\ -\sin(\mathbf{n}_k^j, x_k) & \cos(\mathbf{n}_k^j, x_k) \end{bmatrix}$$

in which $\mathbf{n}_k^j$ represents the unit normal to the boundary at the jth collocation point of the kth sub-domain. The matrices $\boldsymbol{\mu}_k$ and $\mathbf{p}_k$, reflecting the characteristics of the material properties, are expressed as

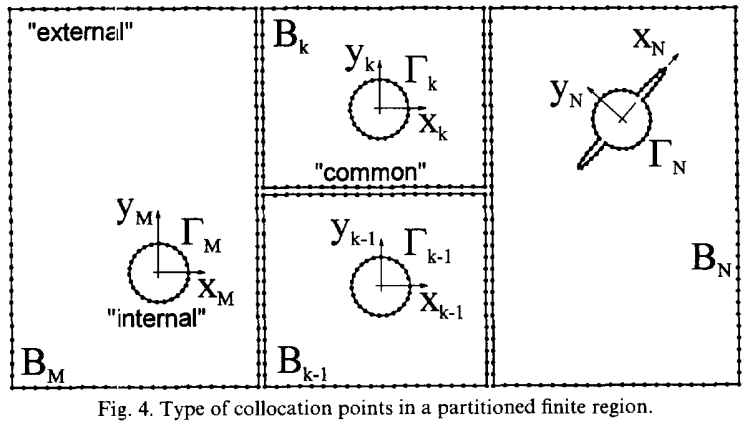

Fig. 4. Type of collocation points in a partitioned finite region.

$$\boldsymbol{\mu}_k = \begin{bmatrix} \mu_{1k}^2 & \mu_{2k}^2 \\ 1 & 1 \\ -\mu_{1k} & -\mu_{2k} \end{bmatrix} \quad \text{and} \quad \mathbf{p}_k = \begin{bmatrix} p_{1k} & p_{2k} \\ q_{1k} & q_{2k} \end{bmatrix} \tag{7}$$

where the variables p_{ik} and q_{ik} are defined by

$$\begin{aligned} p_{ik} &= a_{11}^k \mu_{ik}^2 + a_{12}^k - a_{16}^k \mu_{ik} \\ q_{ik} &= a_{12}^k \mu_{ik} + a_{22}^k / \mu_{ik} - a_{26}^k \end{aligned} \tag{8}$$

and μ_{ik} are the roots of the characteristic equation for the kth sub-domain given by

$$a_{11}^k \mu_k^4 - 2a_{16}^k \mu_k^3 + (2a_{12}^k + a_{66}^k)\mu_k^2 - 2a_{26}^k \mu_k + a_{22}^k = 0. \tag{9}$$

For physically acceptable values of the compliance coefficients, a_{ij}^k, the roots of the characteristic equation are either distinct or equal to their complex conjugates. The in-plane laminate compliance coefficients, a_{ij}^k $(i,j = 1,2,6)$, relating the stress and strain components in the kth sub-domain as

$$\begin{Bmatrix} \varepsilon_{xx} \\ \varepsilon_{yy} \\ \varepsilon_{xy} \end{Bmatrix}_k = \begin{bmatrix} a_{11} & a_{12} & a_{16} \\ a_{12} & a_{22} & a_{26} \\ a_{16} & a_{26} & a_{66} \end{bmatrix}_k \begin{Bmatrix} \sigma_{xx} \\ \sigma_{yy} \\ \sigma_{xy} \end{Bmatrix}_k \quad \text{or } \boldsymbol{\varepsilon}_k = \mathbf{a}_k \boldsymbol{\sigma}_k \tag{10}$$

can be expressed in terms of the elastic constants, E_L, E_T, G_{LT} and v_{LT}, defined in the material coordinate system. The fiber orientation angle, θ_k, is defined relative to the x_k-axis. The subscripts L and T denote the longitudinal and transverse directions relative to the fibers. For the anisotropic kth sub-domain with N layers, the compliance coefficients are established from

$$\mathbf{a}_k = \mathbf{A}_k^{-1} \quad \text{with } A_{ij} = \sum_{n=1}^{N} \bar{\mathcal{Q}}_{ij}^{(n)} t^{(n)} \tag{11}$$

in which $t^{(n)}$ is the thickness of the nth lamina and $\mathcal{Q}_{ij}^{(n)}$ relates the stress and strain components for the nth orthotropic lamina referenced to the coordinate system (x_k, y_k).

The matrix $\boldsymbol{\phi}_k$, whose derivative is denoted by $\boldsymbol{\phi}_k'$, is defined as

$$\boldsymbol{\phi}_k = \begin{bmatrix} \boldsymbol{\phi}_{1k}^{\mathrm{T}} & \mathbf{0} \\ \mathbf{0} & \boldsymbol{\phi}_{2k}^{\mathrm{T}} \end{bmatrix} \tag{12}$$

where

$$\boldsymbol{\phi}_{lk}^{\mathrm{T}} = \{\xi_{lk}^{-N}, \ldots, \xi_{lk}^{-1}, \ln \xi_{lk}, \xi_{lk}, \ldots, \xi_{lk}^{N}\} \quad \text{with } l = 1,2$$

in which ξ_{1k} and ξ_{2k} are the functions mapping the internal boundary to a unit circle and the outer boundary of the sub-domain to the exterior of the unit circle. In the case of a circular internal boundary, the mapping functions are expressed as

$$\xi_{lk} = \frac{z_{lk} \pm \sqrt{z_{lk} - a_k^2 - \mu_{lk}^2 a_k^2}}{a_k - i\mu_{lk}} \quad \text{with } l = 1,2 \tag{13}$$

in which a_k denotes the radius of the kth fastener hole and $i = \sqrt{-1}$. As given by Bowie (1956), these functions become

$$\xi_{lk} = \frac{z_{lk}}{a_k + c_k} \pm \sqrt{\left(\frac{z_{lk}}{a_k + c_k}\right)^2 - 1} \quad \text{with } l = 1, 2 \tag{14}$$

for a hole with two radial edge cracks of length c_k. The complex characteristic coordinates for the kth sub-domain, z_{1k} and z_{2k}, are defined by

$$z_{lk} = x_k + \mu_{lk} y_k \quad \text{with } l = 1, 2. \tag{15}$$

The constant matrices $\mathbf{l}$ and $\mathbf{m}$ are defined by

$$\mathbf{l} = \begin{bmatrix} 1 & 0 & 0 \\ 0 & 1 & 0 \end{bmatrix} \quad \text{and} \quad \mathbf{m} = \begin{bmatrix} 1 & 0 & 1 \\ 0 & 1 & -i \end{bmatrix}. \tag{16}$$

The vector $\boldsymbol{\chi}_k$ consists of the unknown coefficients represented by α_k, β_k, γ_k and Δ_k as

$$\boldsymbol{\chi}_k^{\mathrm{T}} = \{\boldsymbol{\alpha}_k^{\mathrm{T}}, \boldsymbol{\beta}_k^{\mathrm{T}}, \gamma_k, \Delta_k\} \tag{17}$$

in which

$$\boldsymbol{\alpha}_k^{\mathrm{T}} = \{\alpha_{-Nk}, \ldots, \alpha_{-1k}, \alpha_{0k}, \alpha_{1k}, \ldots, \alpha_{Nk}\} \tag{18}$$

and

$$\boldsymbol{\beta}_k^{\mathrm{T}} = \{\beta_{-Nk}, \ldots, \beta_{-1k}, \beta_{0k}, \beta_{1k}, \ldots, \beta_{Nk}\}.$$

The unknown complex coefficients, α_{ik}, β_{ik}, γ_k and Δ_k, are determined by enforcing the boundary conditions at the collocation points on the boundary (Fig. 4). The unknown complex coefficient, γ_k, permits rigid-body translation of the sub-domain. Therefore, additional displacement constraints are required as boundary conditions to prevent rigid-body movement. In order to impose the boundary and constraint conditions associated with the boundary of the fastener hole within the scheme of a boundary collocation formulation, the components of the kth fastener displacement are expressed as an unknown complex variable,

$$\Delta_k = \Delta_{xk} + i\Delta_{yk}. \tag{19}$$

Based on the solution for a pin-loaded infinitely large anisotropic plate given by Lekhnitskii (1968), the components of the force, $\mathbf{F}_k$, exerted by the kth fastener on the hole boundary are represented as

$$\begin{aligned} F_{xk} &= \mathrm{Re}\,[4\pi i(\mu_{1k}\alpha_{0k} + \mu_{2k}\beta_{0k})] \\ F_{yk} &= \mathrm{Re}\,[4\pi i(\alpha_{0k} + \beta_{0k})]. \end{aligned} \tag{20}$$

The continuity of stress and displacement components at the ith and jth "common" collocation points of the $(k-1)$th and kth sub-domains, respectively (Fig. 4), is enforced as

$$\begin{aligned} \mathbf{u}_{k-1}(x_{k-1}^i, y_{k-1}^i) - \mathbf{u}_k(x_k^j, y_k^j) &= 0 \\ \boldsymbol{\sigma}_{k-1}(x_{k-1}^i, y_{k-1}^i) - \boldsymbol{\sigma}_k(x_k^j, y_k^j) &= 0. \end{aligned} \tag{21}$$

The conditions for single-valued displacement components, expressed as

$$\begin{aligned} \mathrm{Im}\,[p_{1k}\alpha_{0k} + p_{2k}\beta_{0k}] &= 0 \\ \mathrm{Im}\,[q_{1k}\alpha_{0k} + q_{2k}\beta_{0k}] &= 0 \end{aligned} \tag{22}$$

along with the boundary conditions at each collocation point, result in an over-determined system of algebraic equations in the form

$$\mathrm{Re}\,[\mathbf{C}\chi] = \mathbf{b} \tag{23}$$

where the matrix $\mathbf{C}$ is composed as

$$\mathbf{C} = \begin{bmatrix} \mathbf{C}_\Delta^1 & \mathbf{C}^1 & 0 \\ \mathbf{C}_\Delta^2 & 0 & \mathbf{C}^2 \end{bmatrix} \tag{24}$$

in which the complex sub-matrix $\mathbf{C}^p$, of order $2(M_1+,\ldots,+M_K)$ by $K(4N+3)$, represents the terms associated with the unknown coefficients in vector χ^p of the pth region, with $p = 1, 2$ corresponding to the upper and lower laminates. The coupling sub-matrices, $\mathbf{C}_\Delta^p$, arise because of the unknown fastener displacements, Δ_k^p, common to both the upper and lower laminates (regions). The unknown vector, χ, in eqn (23) becomes

$$\chi = \begin{Bmatrix} \chi_\Delta \\ \chi^1 \\ \chi^2 \end{Bmatrix} \tag{25}$$

with χ^p defined as

$$\chi^{p^{\mathrm{T}}} = \{\chi_1^{p^{\mathrm{T}}}, \chi_2^{p^{\mathrm{T}}}, \ldots, \chi_K^{p^{\mathrm{T}}}\} \tag{26}$$

in which $\chi_k^{p^{\mathrm{T}}}$ is given by eqn (17) for each region. The vector χ_Δ consists of the unknown fastener displacements. Also, in eqn (23), the known vector, $\mathbf{b}$, of order $4(M_1+,\ldots,+M_K)$ and containing the prescribed boundary conditions, is expressed as

$$\mathbf{b} = \begin{Bmatrix} \mathbf{b}^1 \\ \mathbf{b}^2 \end{Bmatrix}. \tag{27}$$

The number of collocation points associated with the kth sub-domain is denoted by M_k and K is the total number of sub-domains in the region.

Imposition of the condition for single-valued displacement components given by eqn (22) permits the determination of β_{0k} in terms of α_{0k}, thus leading to the modification of $\mathbf{C}$ and χ in eqn (23) through the elimination of β_{0k}. The modified forms of the matrix $\mathbf{C}$ and χ are represented by $\mathbf{C}^*$ and χ^*, resulting in

$$\mathrm{Re}\,[\mathbf{C}^*\chi^*] = \mathbf{b}. \tag{28}$$

In order to perform the numerical calculations with real variables, this system of equations is rewritten as

$$\mathbf{Dd} = \mathbf{b} \tag{29}$$

where the real matrix $\mathbf{D}$, of size $4(M_1+,\ldots,+M_K)$ by $4K(4N+2)$, and the real vector $\mathbf{d}$, of size $4K(4N+2)$, are defined as

$$\mathbf{D} = [\bar{\mathbf{C}}^* - \bar{\bar{\mathbf{C}}}^*] \quad \text{and} \quad \mathbf{d} = [\bar{\chi}^* \bar{\bar{\chi}}^*]$$

in which

$$\bar{\mathbf{C}}^* = \mathrm{Re}\,[\mathbf{C}^*] \quad \text{and} \quad \bar{\bar{\mathbf{C}}}^* = \mathrm{Im}\,[\mathbf{C}^*]$$

$$\bar{\boldsymbol{\chi}}^* = \mathrm{Re}\,[\boldsymbol{\chi}^*] \quad \text{and} \quad \bar{\bar{\boldsymbol{\chi}}}^* = \mathrm{Im}\,[\boldsymbol{\chi}^*].$$

The solution to this over-determined system of equations (29) can be obtained through either the least-squares procedure in conjunction with the Gauss elimination method or the singular value decomposition method. However, the matrix **D** may be ill-conditioned if the collocation points are subject to mixed boundary conditions involving both the displacement constraints and tractions, which may differ in value by orders of magnitude. Therefore, the norm of each row in **D** is scaled by pre-multiplying the system of equations (29) with a matrix, **S**, resulting in

$$\mathbf{D}_s\mathbf{d} = \mathbf{b}_s \tag{30}$$

where

$$\mathbf{D}_s = \mathbf{SD} \quad \text{and} \quad \mathbf{b}_s = \mathbf{Sb}$$

in which

$$S_{ij} = s_i\delta_{ij} \quad \text{with } i,j = 1, 2(M_1+,\ldots,+M_K).$$

Based on an extensive numerical experimentation, the scaling parameters, s_i, are assigned a value of unity and E_n/Z_i for collocation points involving traction conditions and displacement constraints, respectively. The parameter E_n is the Young's modulus of the material in the direction normal to the boundary, and Z_i is the distance between the ith collocation point and the origin of the coordinate system.

The solution by the least-squares procedure requires the pre-multiplication of eqn (30) by $\mathbf{D}_s^{\mathrm{T}}$, resulting in

$$\mathbf{D}^*\mathbf{d} = \mathbf{b}^* \tag{31}$$

where the symmetric matrix, $\mathbf{D}^*$, with full rank and $\mathbf{b}^*$ are given by

$$\mathbf{D}^* = \mathbf{D}_s^{\mathrm{T}}\mathbf{D}_s \quad \text{and} \quad \mathbf{b}^* = \mathbf{D}_s^{\mathrm{T}}\mathbf{b}_s.$$

Employing the Gauss elimination method yields the solution to eqn (31) after approximately $[K(4N+2)]^3/3$ number of operations while requiring the storage of $(4N+2)/2(4N+3)$ numbers.

The solution to eqn (30) by singular value decomposition in the sense of a least squares approximation is obtained as

$$\mathbf{d} = \mathbf{VWU}^{\mathrm{T}}\mathbf{b}_s \tag{32}$$

where **V** is the orthogonal matrix of size $2K(4N+2)$ by $2K(4N+2)$; **W** is a diagonal matrix of size $2K(4N+2)$ by $2K(4N+2)$ consisting of singular values, w_i; and **U** is the column orthogonal matrix of size $2(M_1+,\ldots,+M_2)$ by $2K(4N+2)$. As part of the solution, the ratio of largest to smallest singular values can be used as an indicator for the condition of the matrix. The matrix becomes ill-conditioned for large ratios. This solution method requires the storage of $(M_1+,\ldots,+M_K)\times K(4N+2)$ entries of the matrix $\mathbf{D}_s$ and about $2(M_1+,\ldots,+M_K)\times[K(4N+2)]^2+4[K(4N+2)]^3$ number of operations. Although very powerful, this method loses its effectiveness for matrices with a much larger number of rows than columns.

Solving for **d** in eqn (30), by either of these methods, yields unknown coefficients, thus permitting the pointwise calculation of stress and displacement components in the region. Comparison of these calculations with the prescribed boundary conditions establishes the accuracy of the analysis. The error associated with the stress and displacement components, E_σ and E_u, respectively, is quantified in the sense of a root mean square as

$$E_\sigma = \left\{\frac{1}{L_1}\sum_{l=1}^{L_1}[\sigma_k(x_k^l, y_k^l) - \sigma_k^*(x_k^l, y_k^l)]^2 + \frac{1}{L_2}\sum_{l=1}^{L_2}[\tau_k(x_k^l, y_k^l) - \tau_k^*(x_k^l, y_k^l)]^2\right\}^{1/2} \tag{33a}$$

$$E_u = \left\{\frac{1}{L_3}\sum_{l=1}^{L_3}[u_k(x_k^l, y_k^l) - u_k^*(x_k^l, y_k^l)]^2 + \frac{1}{L_4}\sum_{l=1}^{L_4}[v_k(x_k^l, y_k^l) - v_k^*(x_k^l, y_k^l)]^2\right\} \tag{33b}$$

for the "external" and "internal" collocation points. The superscript * denotes the prescribed values of the normal and tangential stress and displacement components. For the "common" collocation points, these expressions are modified in the form

$$E_\sigma = \left\{\frac{1}{L_1}\sum_{l=1}^{L_1}[\sigma_{k-1}(x_{k-1}^l, y_{k-1}^l) - \sigma_k(x_k^l, y_k^l)]^2 + \frac{1}{L_2}\sum_{l=1}^{L_2}[\tau_{k-1}(x_{k-1}^l, y_{k-1}^l) - \tau_k(x_k^l, y_k^l)]^2\right\}^{1/2} \tag{34a}$$

$$E_u = \left\{\frac{1}{L_3}\sum_{l=1}^{L_3}[u_{k-1}(x_{k-1}^l, y_{k-1}^l) - u_k(x_k^l, y_k^l)]^2 + \frac{1}{L_4}\sum_{l=1}^{L_4}[v_{k-1}(x_{k-1}^l, y_{k-1}^l) - v_k(x_k^l, y_k^l)]^2\right\}^{1/2}. \tag{34b}$$

The parameters L_i, with $i = 1, 4$, denote the total number of collocation points involving boundary conditions on the normal and tangential stress and displacement components, respectively.

After invoking the constraint conditions (4) concerning the components of the fastener forces into the resulting linear system of equations (23), its solution subject to the constraint conditions (3) is obtained through an iterative scheme. The iterative scheme begins with the initial estimate of the angles η_{1k}^p and ψ_{1k}^p defining the slip zone and η_{2k}^p and ψ_{2k}^p defining the no-slip zone of the contact region associated with the kth fastener in the pth region. If the constraint conditions specified in eqn (3) are not satisfied, these angles are adjusted by examining the variation of the stress and displacement fields along the hole boundary. When the constrain condition associated with the collocation point is violated, the nature of the boundary conditions is changed in order to eliminate the constraint violation. In correcting the boundary conditions, the collocation points located in the non-contact region, contact regions, and its no-slip zone are examined for the presence of no overlap between the fastener and the hole boundary, compressive stress, and no slip. For the collocation point located in the non-contact region, the condition of no overlap requires that

$$u_k^p(a_k, \theta_k) - (\Delta_{x\kappa}^p \cos\theta_k + \Delta_{yk}^p \sin\theta_k - \lambda_k) < 0. \tag{35}$$

If the collocation point is associated with the correct region, the condition of compressive normal stress is satisfied by

$$\sigma_k^p(a_k, \theta_k) < 0. \tag{36}$$

In the presence of friction, for the collocation point located in the no-slip zone of the contact region, the condition of no slip is applied as

$$\tau_k^p(a_k, \theta_k) < f|\sigma_k^p(a_k, \theta_k)|. \tag{37}$$

This process continues until the variation of the angles describing the contact region is confined to a few collocation points. The converged solution provides the stress and displacement field within each region and, thereby, the forces exerted by each fastener through the integration of contact stresses over the contact region.

The solution to the unknown coefficients associated with each region, α_{ik}^p, β_{ik}^p, γ_k^p and Δ_k^p, yields the explicit expressions for the analytic functions $\Phi_{1k}^p(z_{1k})$ and $\Phi_{2k}^p(z_{2k})$ expressed in the truncated series form in terms of the mapping functions ξ_{1k} and ξ_{2k} as

$$\Phi_{1k}^p(\xi_{1k}) = \alpha_{0k}^p \ln \xi_{1k} + \sum_{n=1}^{N} (\alpha_{-nk}^p \xi_{1k}^{-n} + \alpha_{nk}^p \xi_{1k}^n)$$

$$\Phi_{2k}^p(\xi_{2k}) = \beta_{0k}^p \ln \xi_{2k} + \sum_{n=1}^{N} (\beta_{-nk}^p \xi_{2k}^{-n} + \alpha_{nk}^p \xi_{2k}^n) \tag{38}$$

leading to the expressions for the stress and displacement components in the kth sub-domain of the pth region

$$\begin{aligned}
\sigma_{xx}^k &= 2\,\mathrm{Re}\,[\mu_{1k}^{p2}\Phi_{1k}^{p'}(z_{1k}) + \mu_{2k}^{p2}\Phi_{2k}^{p'}(z_{2k})] \\
\sigma_{yy}^k &= 2\,\mathrm{Re}\,[\Phi_{1k}^{p'}(z_{1k}) + \Phi_{2k}^{p'}(z_{2k})] \\
\sigma_{xy}^k &= -2\,\mathrm{Re}\,[\mu_{1k}^{p}\Phi_{1k}^{p'}(z_{1k}) + \mu_{2k}^{p}\Phi_{2k}^{p'}(z_{2k})] \\
u_x^k &= 2\,\mathrm{Re}\,[p_{1k}^{p}\Phi_{1k}^{p}(z_{1k}) + p_{2k}^{p}\Phi_{2k}^{p}(z_{2k}) + \gamma_k^p] \\
u_y^k &= 2\,\mathrm{Re}\,[q_{1k}^{p}\Phi_{1k}^{p}(z_{1k}) + q_{2k}^{p}\Phi_{2k}^{p}(z_{2k}) - i\gamma_k^p]
\end{aligned} \tag{39}$$

in which a prime denotes differentiation with respect to the corresponding argument. For a line crack or inclusion in the kth sub-domain, the stress intensity factors K_{I} and K_{II} are obtained directly as defined by Sih *et al.* (1965)

$$K_{\mathrm{I}}^k + \frac{K_{\mathrm{II}}^k}{\mu_{2k}} = 2\sqrt{2\pi}\,\frac{\mu_{2k}-\mu_{1k}}{\mu_{2k}} \lim_{z_{1k}\to z_k^*} \sqrt{z_{1k}-z_k^*}\,\Phi_{1k}(z_{1k}) \tag{40}$$

in which z_k^* refers to the crack tip.

NUMERICAL RESULTS

This study presents numerical results for two different joint configurations in order to establish the generality of the present approach. Validation of the present method can be found in a report by Madenci *et al.* (1996). The first configuration concerns a composite laminate fastened to an aluminum plate with eight uniformly distributed fasteners. Because of the presence of symmetry, only half of the joint with four fasteners is explicitly considered (Fig. 5). Each fastener has a radius of $a_k = 3$ mm, with fastener-hole clearance of $\lambda_k = 0$

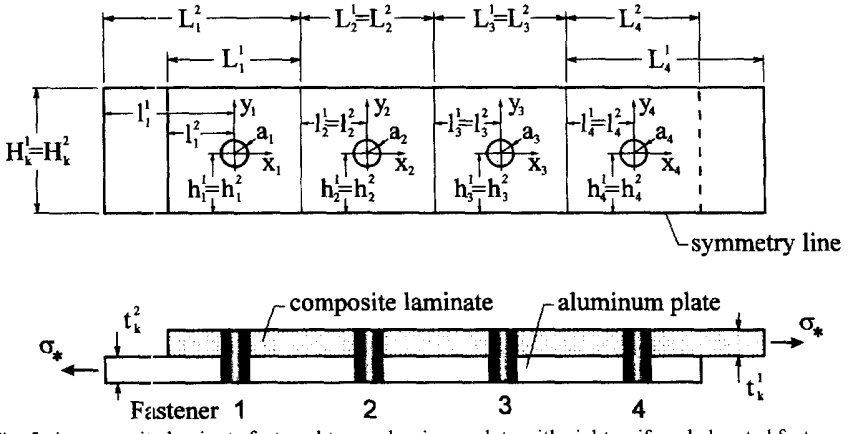

Fig. 5. A composite laminate fastened to an aluminum plate with eight uniformly located fasteners.

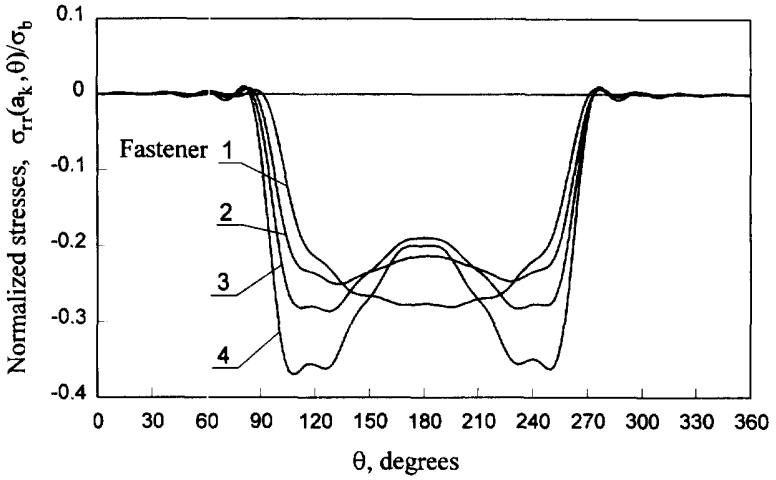

Fig. 6. Radial stress distribution along the fastener-hole boundaries in the composite laminate.

($k = 1, 4$). The laminate lay-up is quasi-isotropic $[(\pm 45/0/90)_3]_s$ with $E_L = 147$ GPa, $E_T = 11$ GPa, $G_{LT} = 5.3$ GPa, and $v_{LT} = 0.3$. The compliance of a titanium fastener is computed using eqn (1) with $E_k = 110$ GPA and $v_k = 0.29$. The dimensions of the sub-domains in the composite laminate and the aluminum plate are specified by $L_1^1 = L_4^2 = 30$ mm, $L_4^1 = L_1^2 = 44.5$ mm, $L_\alpha^p = 30$ mm ($p = 1, 2$ and $k = 2, 3$), and $H_k^p = 28.5$ mm, and their thickness is $t_k^p = 3.046$ mm ($p = 1, 2$ and $k = 1, 4$). The positions of the fasteners in relation to the boundaries of each region are given by $h_k^p = 13.5$ mm ($p = 1, 2$ and $k = 1, 4$) and $l_k^p = 15$ mm ($p = 1, 2$ and $k = 1, 4$, with $k \neq 1$ and $p \neq 2$), and $l_1^2 = 29.5$ mm. The aluminum plate and the laminate at the free ends are subjected to a uniform stress of $\sigma_* = 28.8$ MPa. Each of the regions includes 344 collocation points, 164 and 180 along the external and hole boundaries, respectively. The number of terms in series representation, N, is equal to 10, leading to a total of 6082 unknowns in the system of equations (30). In the absence of friction, the variation of the normalized radial and circumferential stresses, $\sigma_{rr}(a_k, \theta)/\sigma_b$ and $\sigma_{\theta\theta}(a_k, \theta)/\sigma_b$, with $\sigma_b = \sigma_* H_k^p/2a_k$ along the boundaries of the fastener holes in both the aluminum and the composite plate is shown in Figs 6–9. It is apparent from the figures that the usual assumption of cosinusoidal radial (bearing) stress distributions is

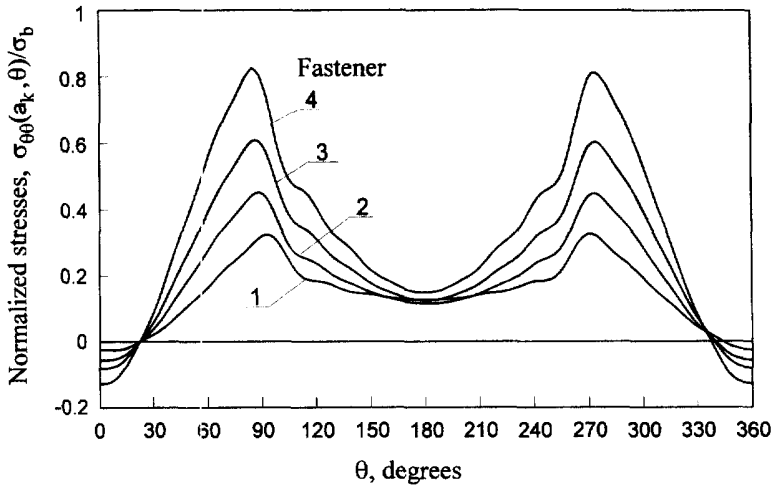

Fig. 7. Circumferential stress distribution along the fastener-hole boundaries in the composite laminate.

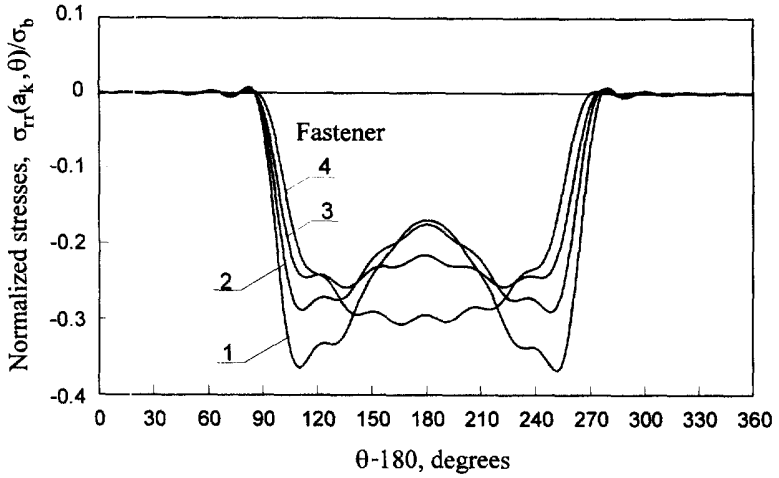

Fig. 8. Radial stress distribution along the fastener-hole boundaries in the aluminum plate.

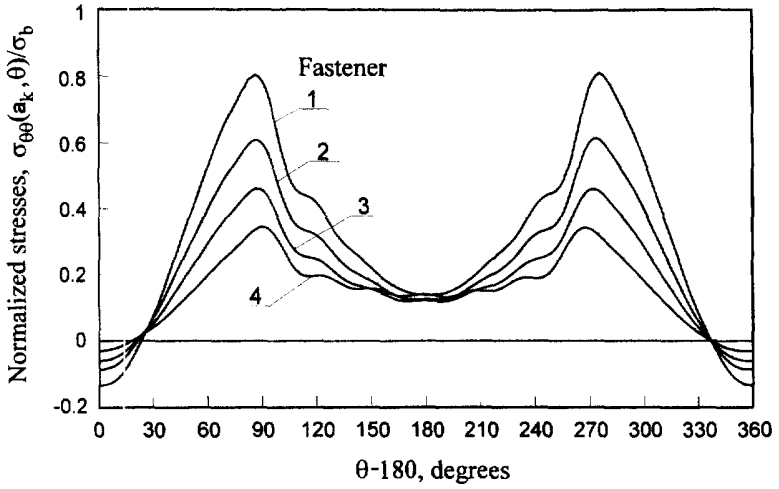

Fig. 9. Circumferential stress distribution along the fastener-hole boundaries in the aluminum plate.

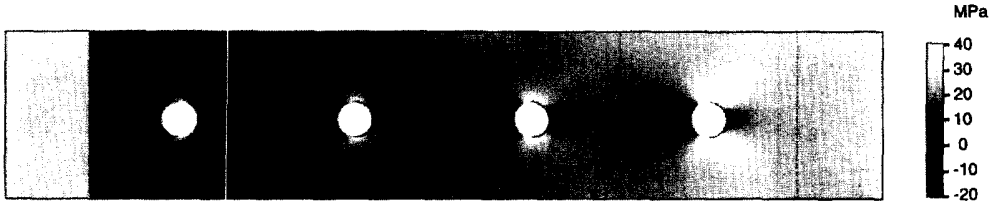

Fig. 10. Variation of the normal stress along the loading direction in the composite laminate.

not valid for all the fasteners. For fasteners near the loaded ends, the peak radial and circumferential stresses increase significantly. The nature of the interaction among the fasteners is described in Fig. 10 by the variation of the normal stress in the x-direction. The loads exerted by each fastener are computed to be $F_{x1} = 631$ N, $F_{y1} = 14$ N, $F_{x2} = 566$ N, $F_{y2} = 2$ N, $F_{x3} = 528$ N, $F_{y3} = -7$ N, $F_{x4} = 681$ N, and $F_{y4} = -20$ N. The contact region associated with each fastener is established by the computed angles of ψ^p_{2k} and η^p_{2k}, and the

Table 1. Angles specifying the contact region for each fastener (degrees)

	Fastener number							
	1		2		3		4	
	ψ_2	η_2	ψ_2	η_2	ψ_2	η_2	ψ_2	η_2
Composite laminate	84	90	90	90	90	90	90	88
Aluminum plate	90	92	90	90	90	90	90	88

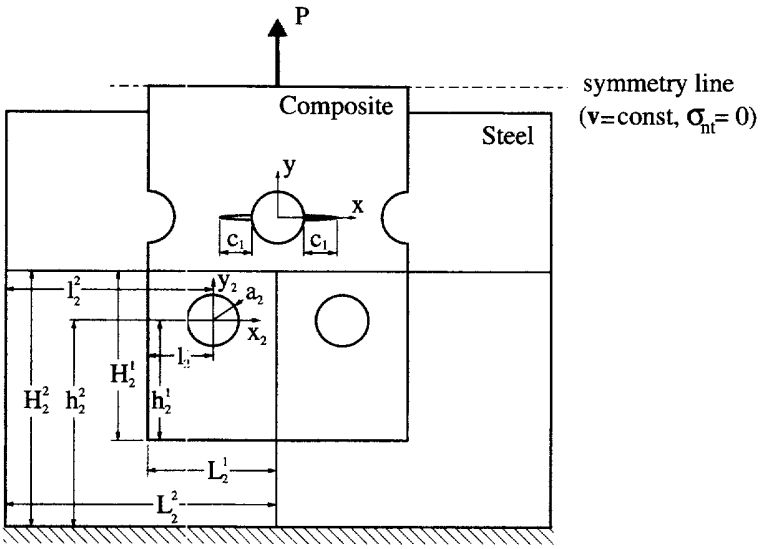

Fig. 11. A composite laminate with edge cracks, fastened to a steel plate with staggered fasteners.

results are presented in Table 1. The non-symmetrical contact regions occur because of the fastener forces exerted in the y-direction.

The second configuration concerns a composite laminate fastened to a steel plate with three fasteners (Fig. 11). The laminate lay-up is $[0_{10}^{\circ}/\pm 45_4^{\circ}/90_2^{\circ}]$ with $E_L = 202.75$ GPa, $E_T = 6.97$ GPa, $G_{LT} = 5.27$ GPa, and $v_{LT} = 0.26$. Each fastener hole has a radius of $a_k = 9.529$ mm, with a fastener-hole clearance of $\lambda_k = 0$ $(k = 1, 3)$. The fasteners are assumed to be rigid. The dimensions of the sub-domains in the steel plate are specified by $H_1^2 = 57.2$ mm, $L_1^2 = 200.025$ mm, $H_2^2 = 95.3$ mm, and $L_2^2 = 100.0125$ mm, and their thickness is $t_k^2 = 25.4$ mm. The positions of the fasteners in relation to the boundaries of each region are given by $h_1^2 = 19.0$ mm, $l_1^2 = 100.0125$ mm, $h_2^2 = 76.2$ mm, and $l_2^2 = 76.2$ mm. The dimensions of the sub-domains in the composite laminate are specified by $H_1^1 = 66.625$ mm, $L_1^1 = 95.25$ mm, $H_2^1 = 63.55$ mm, and $L_2^1 = 47.625$ mm, and their thickness is $t_k^1 = 25.4$ mm. The positions of the fasteners in relation to the boundaries of each region are given by $h_1^1 = 19.0$ mm, $l_1^1 = 47.625$ mm, $h_2^1 = 44.45$ mm, and $l_2^1 = 23.8125$ mm. One of the fastener holes in the composite laminate has radial edge cracks perpendicular to the direction of loading, with length c_1. The steel plate is subject to zero displacement constraints at the bottom end, while the laminate is loaded by an integral force, $P = 1.163 \cdot 10^7$ N. In place of a specified stress distribution, a condition of uniform vertical displacements of joints on the symmetry line is imposed. The number of collocation points varies from 404 (164 on the external boundary and 240 on the hole) for the sub-domains in the steel plate, to 1784 (784 on the external boundary, 360 on the hole, and 640 on the cracks) for the sub-domain with cracks in the composite laminate. In order to ensure the accuracy of the numerical results, the number of terms in the series representation, N, is chosen as 40 for the region with the cracks and 15 for other regions. This leads to a total of 9000 unknowns in the governing system of eqns (30). The non-uniform location of the collocation points along the crack is required to obtain accurate results. In reference to the

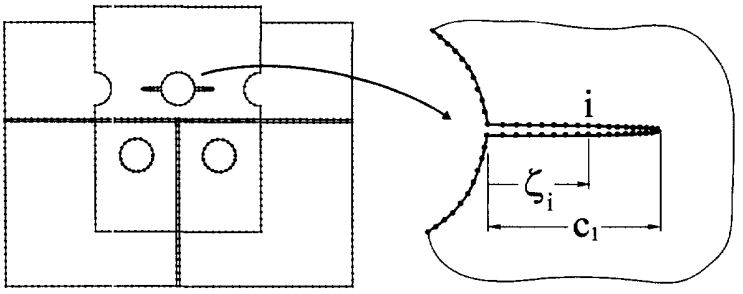

Fig. 12. Collocation points associated with the sub-domains of the composite laminate and the aluminum plate with three fasteners.

Table 2. Comparison of the stress intensity factors obtained from the boundary collocation technique with those from the finite element method (MPa$\sqrt{\text{m}}$)

Crack length, c_1 (mm)	Boundary collocation technique		Finite element method	
	K_I	K_{II}	K_I	K_{II}
3	1338.7	−109.4	1350.2	−131.9
5	1400.3	−90.3	1434.6	−64.2
10	1614.9	22.2	1646.3	−69.7
15	1768.4	62.2	1932.5	−34.7
20	2427.4	11.0	2468.7	−23.6

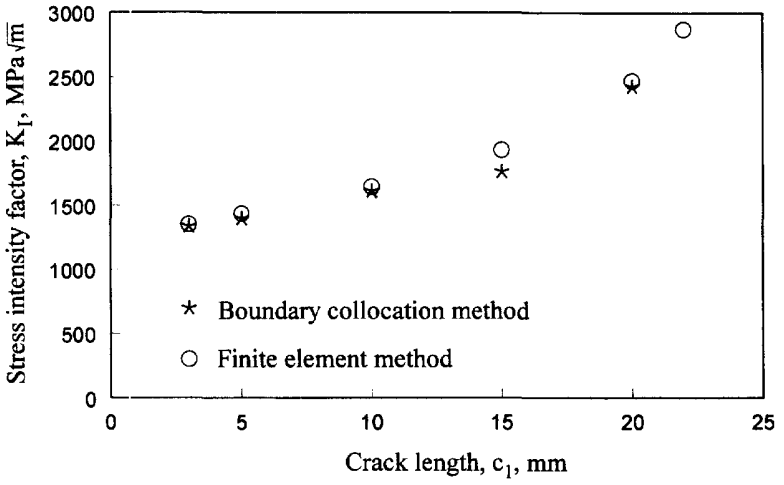

Fig. 13. Variation of the stress intensity factors as a function of the crack length for the opening mode.

hole boundary, as shown in Fig. 12, the location of the collocation points along the crack is determined using

$$\zeta_i = c\frac{1-\rho^{i/M_{1L}-1}}{1-\rho^{L/M_{1L}-1}}$$

where ζ_i denotes the distance from the hole boundary and ρ is the parameter specifying the non-uniform spacing between the collocation points, with $(M_{1L}+i)$ corresponding to the number of the collocation point. The stress intensity factors for different crack lengths are presented in Table 2 and are shown in Fig. 13 in comparison with those obtained by the finite element method. The finite element analysis was conducted by using a modified

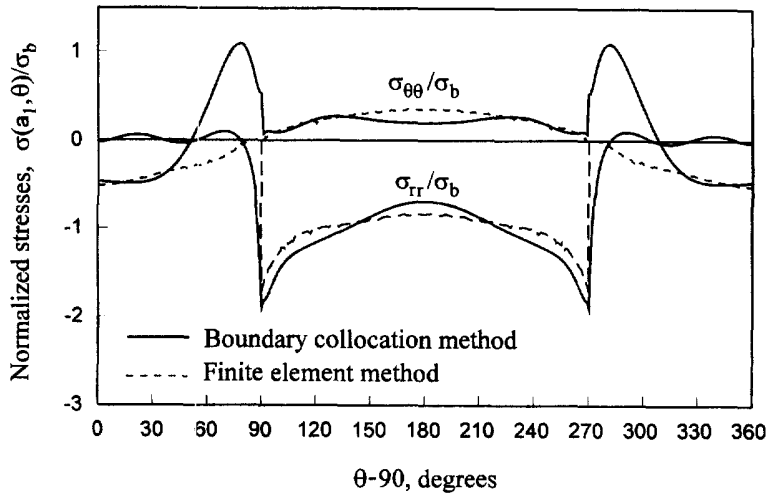

Fig. 14. Stress distribution around the fastener hole with edge cracks in the composite laminate.

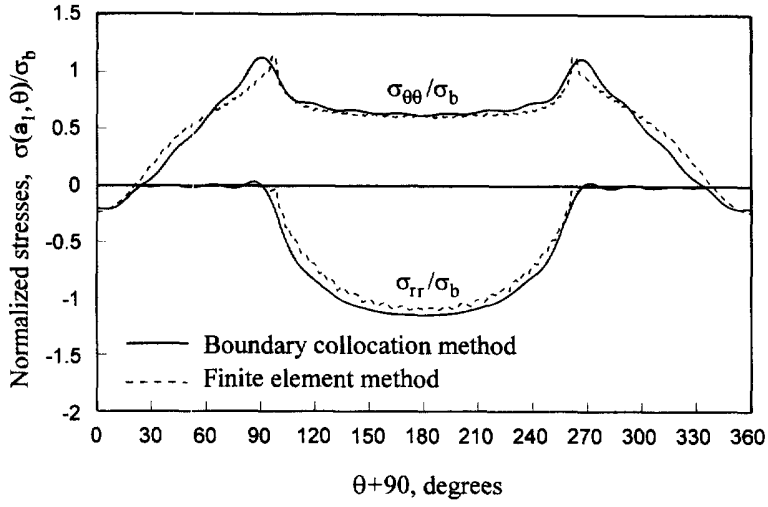

Fig. 15. Stress distribution around the central fastener hole in the steel plate.

version of PAPST, a program originally developed by Hilton and Wilmarth (1982), with 12-noded rectangular and 9-noded triangular isoparametric elements. The contact algorithm is consistent with the preceding procedure described for the boundary collocation technique. Elements of a size less than 1% of the crack length around the crack tip are used in order to capture the singular stress field. The values for the stress intensity factors are obtained by extrapolation from the stresses along the crack line. The variation of the normalized radial and circumferential stresses around the central fastener hole, $\sigma_{rr}(a,\theta)/\sigma_b$ and $\sigma_{\theta\theta}(a,\theta)/\sigma_b$ with $\sigma_b = F_{x_1}/2a_1t_1$, both in the steel and composite plate is shown in Figs 14 and 15. The comparison of the stress variation is favorable, except for the circumferential stresses for the hole boundary with edge cracks in the composite laminate because of the coarse mesh used for the finite element model of the corner (intersection of the crack with the hole boundary). Also the variation of the normal stress in the y-direction (Fig. 16) describes the nature of the interaction among the fasteners. The loads exerted by each fastener are presented in Table 3 for various crack lengths.

CONCLUSIONS

Analytical/numerical investigations concerning the determination of both the contact stresses and the stress intensity factors in mechanical joints with arbitrarily located multiple

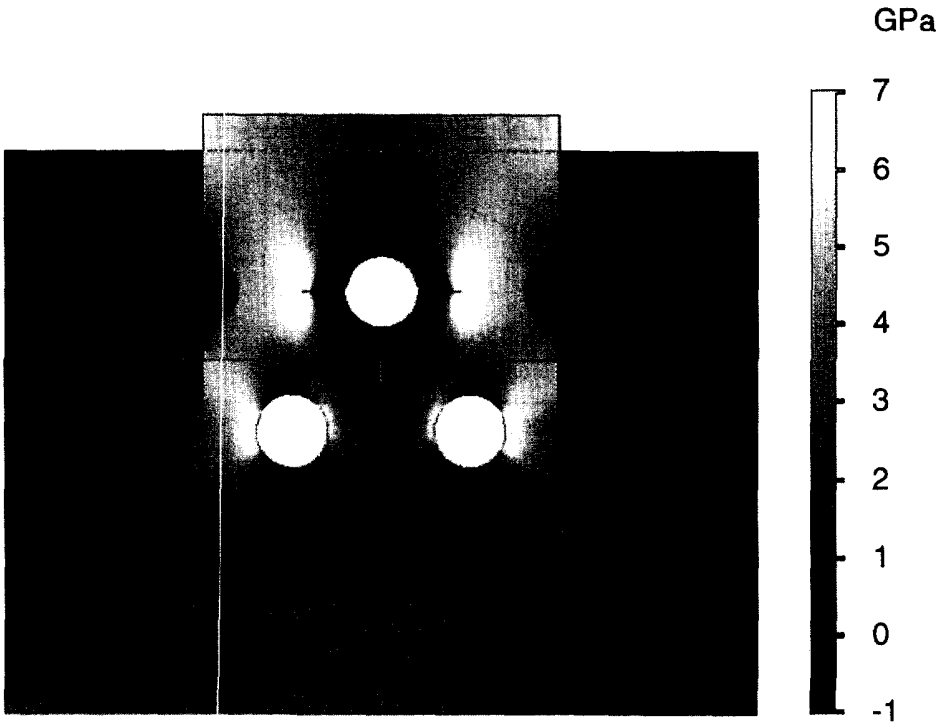

Fig. 16. Variation of the normal stress along the loading direction in the composite laminate.

Table 3. Fastener forces for different crack lengths (N)

Crack length, c_1 (mm)	Left bolt F_X	Left bolt F_Y	Central bolt F_Y
3	106,650	3,694,207	4,349,311
5	100,220	3,825,367	4,197,037
10	170,956	4,120,279	4,002,592
15	269,537	4,468,868	3,767,785
20	245,559	4,658,393	3,657,587

fasteners do not exist in the literature. This study eliminates this discrepancy while synthesizing all of the various effects, such as finite geometry, fastener flexibility, fastener-hole clearance, presence of edge cracks, friction, by-pass loading, and interaction among fasteners, into a comprehensive design/analysis methodology suitable for fast design iterations. Comparison of the results from this analysis with various previous solutions published by others demonstrates the accuracy of the present analysis. This analysis is a significant improvement over the previous analyses in regard not only to mechanically fastened joints, but also stress concentrations in laminates with internal boundaries under general boundary conditions. Also, it provides an accurate stress analysis, essential in predicting the strength of the mechanical joint, by employing certain failure criteria, leading to strength predictions with the test results available in the literature.

REFERENCES

Bowie, O. L. (1956) Analysis of an infinite plate containing radial crack originating at the boundary of an internal circular hole. *Journal of Mathematics and Physics* **35,** 60–71.

Bowie, O. L. and Neal, D. M. (1970) A modified mapping-collocation technique for accurate calculation of stress intensity factors. *International Journal of Fracture Mechanics* **6,** 199–206.

Chiang, Y. J. and Rowlands, R. E. (1991) Finite element analysis of mixed-mode fracture of bolted composite joints. *Journal of Composites Technology and Research* **13,** 227–235.

Eriksson, L. I., Backlund, J. and Moller, P. (1995) Design of multiple-row bolted composite joints under general in-plane loading. *Composites Engineering* **5,** 1051–1068.

Griffin, O. H., Jr, Hyer, M. W., Cohen, D., Shuart, M. J., Yalamanchili, S. R. and Prasad, C. B. (1994) Analysis of multifastener composite joints. *Journal of Spacecraft and Rockets* **31,** 278–284.

Hilton, P. D. and Wilmarth, D. D. (1982) PAPST—revision 2.0; revised documentation and theoretical manual, Report to DTNSRDC.

Hyer, M. W. and Liu, D. (1984) Stresses in pin-loaded plates: photoelastic results. *Journal of Composite Materials* **19,** 138–153.

Lekhnitskii, S. G. (1968) *Anisotropic Plates*. Gordon and Breach Science Publishers, New York.

Madenci, E., Shkarayev, S. and Sergeev, B. (1996) Analysis of composite joints with multiple fasteners. Final Report to Federal Aviation Administration, Contract no. 94-G-029, The University of Arizona, Tucson.

Oplinger, D. W. (1978) On the structural behavior of mechanically fastened joints in composite structures. *Proceedings of a Conference on Fibrous Composites in Structural Design*, San Diego, California, pp. 575–602.

Oplinger, D. W. and Gandhi, K. R. (1974) Stresses in mechanically fastened orthotropic laminates. *Proceedings of the Second Conference on Fibrous Composites in Flight Vehicle Design*, Dayton, Ohio, pp. 813–841.

Rowlands, R. E., Rahman, T. L., Wilkinson, T. L. and Chang, Y. I. (1982) Single- and multiple-bolted joints in orthotropic materials. *Composites* **13,** 273–279.

Sih, G. C., Paris, P. C. and Irwin, G. R. (1965) On cracks in rectilinearly anisotropic bodies. *International Journal of Fracture Mechanics* **1,** 189–203.

Xiong, Y. and Poon, C. (1994) A design model for composite joints with multiple fasteners. Aeronautical Note IAR-AN080, National Research Council, Canada, NRC no. 32165.